Journal of Rock Mechanics and Geotechnical Engineering 14 (2022) 35–49

Contents lists available at ScienceDirect

Journal of Rock Mechanics and Geotechnical Engineering

journal homepage: www.jrmge.cn

Qian Lecture

Soil–atmosphere interaction in earth structures

Yujun Cui

Laboratoire Navier, Ecole des Ponts ParisTech, France

ARTICLE INFO

Article history:
Received 21 September 2021
Received in revised form
18 November 2021
Accepted 21 November 2021
Available online 10 December 2021

Keywords:
Environmental chamber
Soil water evaporation
Suction-based evaporation model
Embankment
Field monitoring
Numerical modeling

ABSTRACT

The soil–atmosphere interaction was investigated through laboratory testing, field monitoring and numerical monitoring. In the laboratory, the soil water evaporation mechanisms were studied using an environmental chamber equipped with a large number of sensors for controlling both the air parameters and soil parameters. Both sand and clay were considered. In case of sand, a dry layer could be formed during evaporation in the near surface zone where the suction corresponded to the residual volumetric water content. The evaporative surface was situated at a depth where the soil temperature was the lowest. In case of clay, soil cracking occurred, changing the evaporative surface from one-dimensional to three-dimensional nature. The suctionbased evaporation model was adapted to take these phenomena into account by adopting a function of dry layer evolution in the case of sand and by adopting a surface crack ratio and a retative humidity ratio in the case of clay. In the field, the volumetric water content, and the suction as well as the runoff were monitored for an embankment constructed with lime/cement treated soils. It appeared that using precipitation data only did not allow a correct description of the variations of volumetric water content and suction inside the soils, the consideration of water evaporation being essential. It was possible to use a correlation between precipiration and runoff. The hydraulic conductivity was found to be a key parameter controlling the variations of volumetric water content and suction. For the numerical modelling, a fully coupled thermohydraulic model was developed, allowing analyzing the changes in temperature, volumetric water content and suction of soil, with the upper boundary conditions at the interface between soil and atmosphere determined using meteorological data. Comparison between simulations and measurements showed the performance of such numerical approach.

1. Introduction

According to IPCC (2014), many extreme weather and climate events have been observed since 1950, including extreme cold/hot temperatures, extreme high sea levels and an increase in heavy precipitation events. Most of these events are related to human activities. Indeed, IPCC (2018) indicated that human-induced warming reached approximately 1 °C above pre-industrial levels in 2017. Note that the period 1850–1900 has been used as an approximation of pre-industrial temperatures. There is substantial evidence that human-induced global warming has led to an increase in the frequency, intensity and/or amount of heavy precipitation events at the global scale, as well as an increased risk of drought. It is worth noting that risks associated with increases in drought frequency and magnitude are projected to be substantially larger at 2 °C than at 1.5 °C.

According to CCR (Caisse Centrale de Réassurance, France) (https://catastrophes-naturelles.ccr.fr/-/002121_sech_2020), on the world scale, the first half of 2020 was the warmest with a mean temperature 1.12 °C above the 1981–2010 average. The January–August 2020 period was the warmest ever observed since the beginning of meteorological measurements with 1.72 °C above the normal in France. The year 2019 was marked by a winter that was generally drier than average, and by a very dry summer until mid-September. The year 2020 was characterized by a winter that was contrasted in terms of precipitation while being extremely mild. The summer, particularly in July and August, was characterized by significant precipitation deficits. For the sixth time in the last decade, the geotechnical drought event represents a major event in 2020.

These extreme weather and climate events can greatly affect buildings and geotechnical constructions. In France, the shallowly

E-mail address: yu-jun.cui@enpc.fr.

Peer review under responsibility of Institute of Rock and Soil Mechanics, Chinese Academy of Sciences.

https://doi.org/10.1016/j.jrmge.2021.11.004

founded buildings of 216 communes in 17 departments were affected by the extensive drought from 1989 to 1990 (Vandangeon, 1992). According to the decree of November 1, 2005, more than 870 communes were considered affected by the 2003 drought. Examination of the affected buildings showed that the differential settlement due to drying and the differential heave due to wetting were the main reasons for the damage of building structures. The similar phenomena were reported for other countries (Biddle, 1983; Driscoll, 1983; Holtz, 1983; Ravina, 1983; Williams and Pidgeon, 1983; Gao, 1995; Allman et al., 1998). Thereby, it is now widely recognized that the drought-related hazards have important economic, environmental and societal impacts, and deserve particular attention.

Basically, the effect of climate effect on geotechnical constructions represents a vast topic involving various disciplines such as geotechnical engineering, geology, hydrology, meteorology, etc. The research methodology can involve laboratory testing, field monitoring, theoretical development and numerical analysis. In this paper, a fundamental study on soil water evaporation using an environmental chamber was first presented. The analysis of the obtained experimental results allowed soil water evaporation models to be developed, for both sand and clay. Then, some field monitoring results in terms of soil thermo-hydraulic responses to varying meteorological conditions were presented, evidencing the significant soil–atmosphere interaction in earth structures such as embankments. Finally, a numerical analysis was presented, showing the possibility of numerically assessing the thermo-hydraulic behavior of geotechnical constructions with consideration of meteorological data.

It is worth noting that most results presented in this paper were published by the author. However, all figures were re-plotted and most results were re-organized. Most importantly, the results were re-interpreted, allowing new conclusions to be drawn.

2. Investigation of soil water evaporation using environmental chamber

In order to analyze the soil–atmosphere interaction in geotechnical constructions, it is important to well understand the main mechanisms related to soil water evaporation. Previous studies showed that soil water evaporation is controlled by both atmospheric and soil conditions. The water evaporation rate was found to be greater at lower air relative humidity, higher air temperature, higher wind speed and stronger solar radiation (Cui and Zornberg, 2008). The water evaporation rate was found to be dependent on soil water retention capacity, hydraulic conductivity, water content or suction, and dry density, as well as water table level (Wilson et al., 1994; Yanful and Choo, 1997; An et al., 2018a).

For clayey soils, cracks can develop upon drying. Several studies focused on the factors affecting the cracking initiation, including soil layer thickness (Nahlawi and Kodikara, 2006), temperature (Tang et al., 2010), wetting/drying cycles (Tang et al., 2011), fines content (Yesiller et al., 2000), etc. As the developed cracks modify the interface between atmosphere and soil in terms of morphology and water content distribution, the soil water evaporation rate is expected to be greatly affected. This was confirmed by Cui et al. (2013) through an evaporation experiment using an environmental chamber.

Therefore, to well investigate the soil water evaporation phenomenon, it appears necessary to well control the atmospheric conditions (relative humidity, temperature, wind speed, etc.) and the soil conditions (initial state, water table level, dry density, etc.). For clayey soils, in addition, it is necessary to monitor the soil cracking. Nevertheless, until now, few experiments were carried out with full control of atmospheric conditions and good monitoring of soil response (Wilson et al., 1997; Yanful et al., 2003). In this study, soil evaporation was investigated on both sand and clay using an environmental chamber which was initially developed by Tang et al. (2009), and then modified by Song et al. (2013). Analysis of the obtained results allowed the development of soil water models for sand and clay, respectively.

2.1. Environmental chamber

The environmental chamber used for evaporation experimentation is shown in Fig. 1. It is an acrylic chamber of 1000 mm long, 800 mm wide and 895 mm high. The chamber was equipped with a distributor for diffusing the air which was previously heated to a certain temperature, a collector for collecting the air after soil water evaporation, and a water supply for controlling the water table using a graduated tube. The soil sample was prepared by compaction to a desired dry density and the thickness of the sample was 250–300 mm. In the test, the air temperature and relative humidity were measured at the inlet of the chamber before the heated air was diffused into the chamber and at the outlet of the chamber in the air collector.

Different sensors were used to monitor the atmospheric and soil conditions, including high-capacity tensiometers for matric suction measurement, ThetaProbes for volumetric water content measurement, temperature sensors (PT1000) for soil temperature measurement, T3111 transmitters for air temperature and relative humidity measurements, and thermistors for air temperature measurement. Sensor Pyropen-D was installed at the chamber cover for measuring the soil surface temperature. A camera (Canon EOS400D) was used for monitoring the morphology of the soil surface (in the case of clay). A flowmeter (MAS-3120) was used for air flow rate measurement and an anemometer (Testo 435-2) was used for the wind speed measurement. More details about this environmental chamber can be found in Song et al. (2013).

2.2. Case of sand

Fontainebleau sand of 2.64 specific gravity was used. In order to investigate the effects of air temperature and air flow rate, two tests (tests 1 and 2) were carried out. The soil sample was prepared by compaction using a manual compactor to a dry unit mass of 1.7 Mg/m^3. Prior to the evaporation test, the soil sample was saturated by

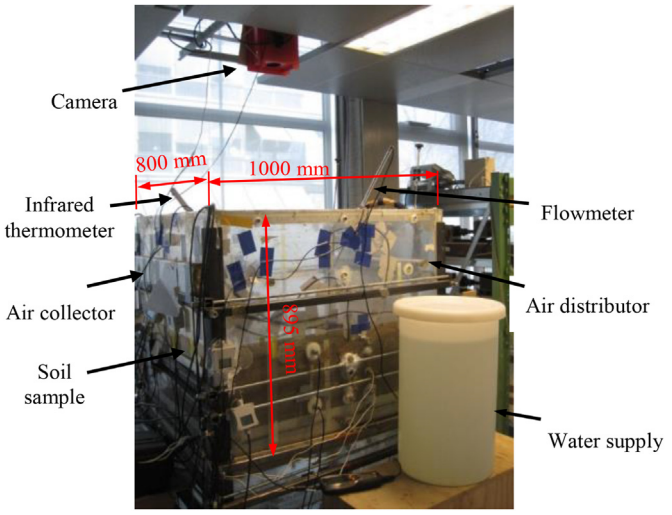

Fig. 1. Environmental chamber used for evaporation experiment (modified from Song et al., 2013).

allowing water infiltration from the bottom. An air temperature of 50 °C in the heating tube and an air flow rate of 185 L/min were applied in test 1, while an air temperature of 200 °C in the heating tube and an air flow rate of 130 L/min were applied in test 2. Note that the temperature in the heating tube was much higher than the temperature of the air diffused in the chamber. Test 1 lasted 11.5 d, while test 2 lasted 30 d.

Fig. 2 shows the air–soil temperature profiles, with some representative selected times (0 d, 4 d, 8 d, and 11.5 d for test 1; and 0 d, 4 d, 8 d, 12 d, and 30 d for test 2). The highest air temperature was obtained at the elevation of air distributor, which was normal because the air was heated in the heating tube before reaching the distributor. The air temperature was decreasing from the distributor to the chamber cover, indicating the room cooling effect. From the distributor to the soil surface, the air temperature was also decreasing. In the case of low heating tube temperature (test 1), the temperature at the soil surface was the lowest (Fig. 2a), while in the case of high heating tube temperature (test 2), this phenomenon was not observed (Fig. 2b). The soil temperature was observed to increase over depth under low heating tube temperature (Fig. 2a), while it decreased slightly under high heating tube temperature (Fig. 2b).

As evaporation is an energy-consuming process, theoretically, the position of the lowest temperature corresponded to the evaporative surface below which there was liquid water and above which there was water vapor only. As in test 1, the soil surface temperature kept the lowest in the whole test duration (11.5 d), it could be deduced that the evaporative surface stayed close to the soil surface. On the contrary, in test 2, the lowest soil temperature was observed at the soil surface only at the beginning of the test; over time, the position of the lowest temperature was found to be deeper, sign of the development of deeper evaporative surface. This suggested the formation of a completely dry layer in the area close to the soil surface in the case of high heating tube temperature (test 2).

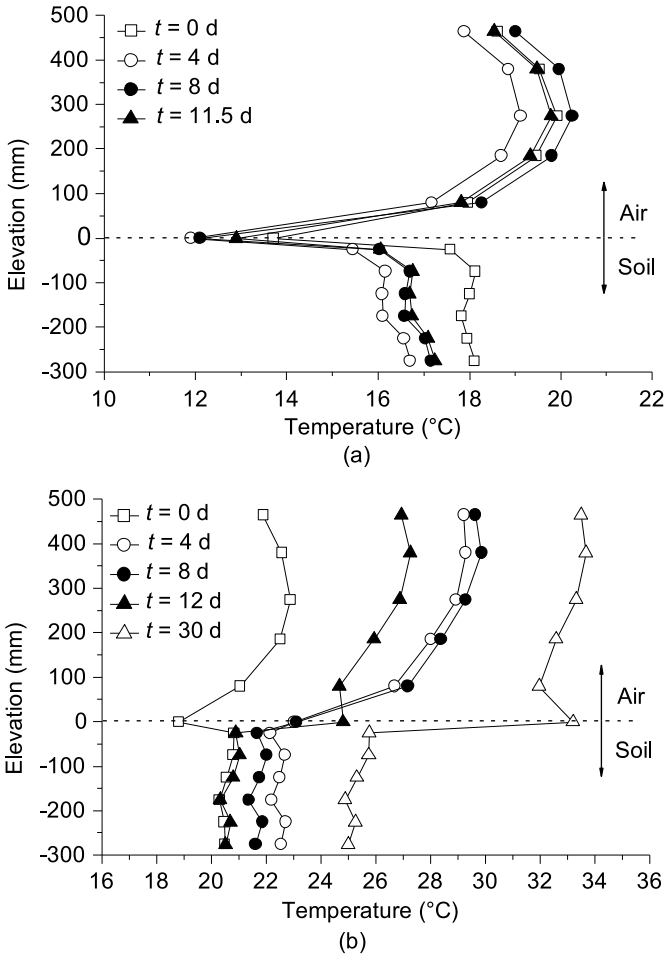

Fig. 2. Temperature profiles in air and soil: (a) Test 1 and (b) test 2 (data from Song et al., 2014).

The air and soil temperatures were found to increase over time. This was because during soil water evaporation, the soil water content decreased and the soil suction increased, leading to a decrease in evaporation rate. As a result, the energy consumed by evaporation declined and more energy was available for heating soil and air.

The profiles of volumetric water content are presented in Fig. 3, with some representative selected times (0 d, 4 d, 8 d, and 11.5 d for test 1; and 0 d, 4 d, 8 d, 12 d, 16 d, and 30 d for test 2). Due to evaporation, the volumetric water content was decreasing significantly in both tests. Further examination showed that water loss occurred mainly in the near surface zone. At depths greater than 275 mm, the water loss was negligible, especially in test 1 with lower heating tube temperature and shorter test duration. Comparison of water loss during about 12 d between test 1 and test 2 showed that the water loss in test 2 was slightly larger, showing the effect of temperature on water evaporation.

The profiles of soil suction are shown in Fig. 4, with some representative selected times (0.25 d, 2 d, 4 d, and 6 d for test 1; and 0 d, 4 d, 8 d, and 16 d for test 2). For test 1, the significant variations occurred in the near surface zone (0–75 mm depth), while for test 2, a large variation in the near surface zone (0–25 mm depth) was followed by a smaller variation in the deeper zone. This suggested a larger influence zone in test 2, in agreement with the observation from Fig. 3 for the volumetric water content variations.

It appeared that the suctions in the near surface zone were higher in test 1 than in test 2, which would suggest more water loss in this zone in test 1. This was contradictory to the results of volumetric water content shown in Fig. 3. A tentative explanation would be related to the soil heterogeneity. Indeed, even though the soil was compacted at the same dry density in both tests, the water flow rates could be different in the two tests, and some fine sand particles would be migrated to the sample surface especially in test 1, leading to higher suctions by evaporation. Note that the sand particle migration is often reported as an internal erosion mechanism (see for instance Chang et al., 2020). This suggested that it should be cautious when further analyzing such data – it would be better to use the mean values of data from different tests.

The data of volumetric water content and suction allowed the water retention curve to be plotted (Fig. 5). Note that in the determination, for each soil suction measurement, the corresponding volumetric water content was determined based on the volumetric water content profiles (see Fig. 3). A large data scatter could be observed, confirming the sample heterogeneity mentioned previously. Fredlund and Xing (1994)'s model can be applied to describe the water retention property of the tested sand:

$$\theta_w = \theta_r + \frac{\theta_s - \theta_r}{\{\ln[e + (\psi/a)^n]\}^m} \quad (1)$$

where θ_w is the volumetric water content (%); θ_s is the volumetric water content in saturated state (θ_s = 35.6%); θ_r is the residual volumetric water content (θ_r = 4%); ψ is the matric suction (kPa); e is the base of natural logarithm (e = 2.71828); and a, n and m are the soil parameters (a = 40, n = 1.4, and m = 15).

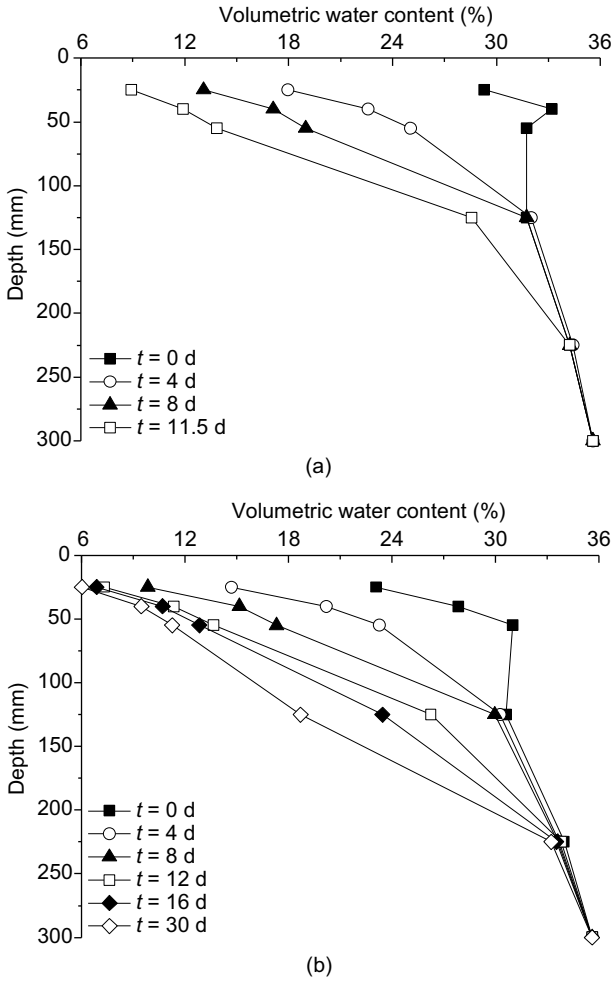

Fig. 3. Volumetric water content profiles: (a) Test 1 and (b) test 2 (data from Song et al., 2014).

The air entry value could be estimated at 1–2 kPa. The suction corresponding to the residual volumetric water content was estimated at 40 kPa. Physically, the residual volumetric water content corresponded to a soil state with discontinuous water phase. In other words, the residual state was close to the completely dry state. Thus, the dry layer mentioned previously for test 2 referred to the soil with suction higher than 40 kPa.

The following equation was used to determine the evaporation rate (Aluwihare and Watanabe, 2003):

$$E_a = 86400 Q_a (H_{a\text{-outlet}} - H_{a\text{-inlet}})/(\rho_l A) \quad (2)$$

where E_a is the actual evaporation rate (mm/d), $H_{a-outlet}$ is the humidity at the outlet (Mg/m^3), $H_{a-inlet}$ is the humidity at the inlet (Mg/m^3), Q_a is the air flow rate through the chamber (L/s), ρ_l is the density of water (Mg/m^3), and A is the area of the evaporative surface (m^2).

The absolute humidity (H_a) is calculated as follows (Aluwihare and Watanabe, 2003):

$$H_a = 0.622 e_a/(1000 R T_a) \quad (3)$$

where T_a is the air temperature (K); R is the gas constant (287.04 J/(kg K)); and e_a is the vapor pressure (Pa), which is calculated as

$$e_a = e_{sat} H_r/100 \quad (4)$$

where H_r is the air relative humidity (%); and e_{sat} is the saturated vapor pressure (Pa), which is calculated using the following equation (Brutsaert, 1988):

$$e_{sat} = 101325 \exp\left(13.3185 t_{R_a} - 1.976 t_{R_a}^2 - 0.6445 t_{R_a}^3 - 0.1299 t_{R_a}^4\right) \quad (5)$$

$$t_{R_a} = 1 - 373.15/T_a \quad (6)$$

Using Eq. (2), the actual evaporation rate was calculated for tests 1 and 2 (Fig. 6). It was observed that during the first 5 d, the evaporation rate in test 1 was between 1.75 mm/d and 2 mm/d, while the evaporation rate in test 2 was about 2 mm/d, indicating that the evaporation rate under low heating tube temperature (test 1) was lower than that under high heating tube temperature (test 2). Moreover, the evaporation rate in test 2 exhibited three-stage variation: (i) a first nearly constant rate, (ii) a second significant declining rate, and (iii) a third stabilized rate. Owing to the short duration of test 1, only one stage was observed.

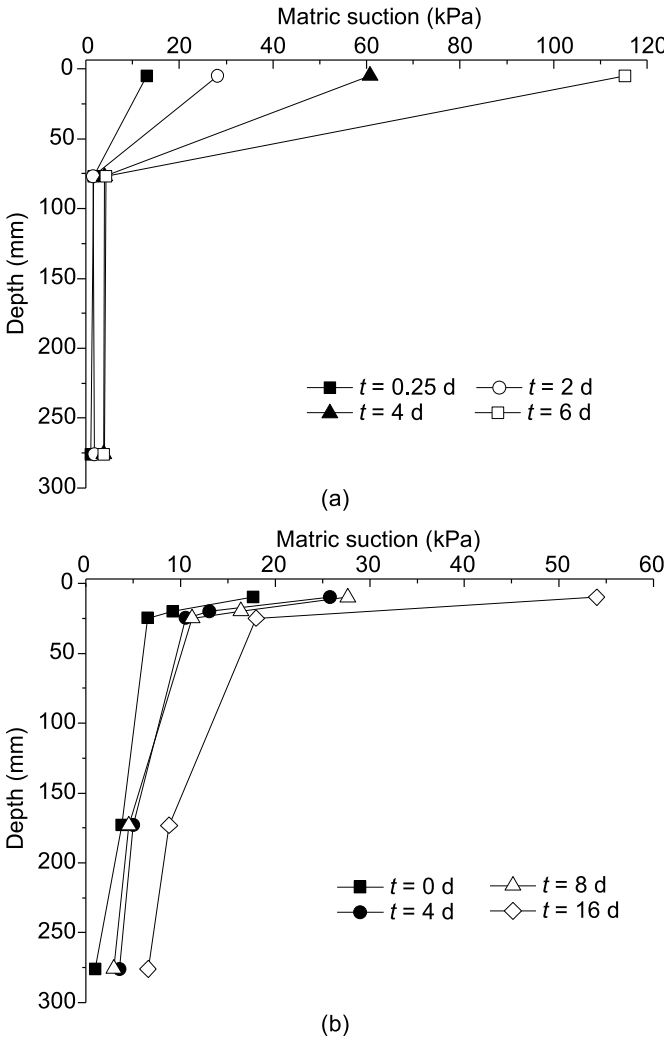

Fig. 4. Profiles of suction: (a) Test 1 and (b) test 2 (data from Song et al., 2014).

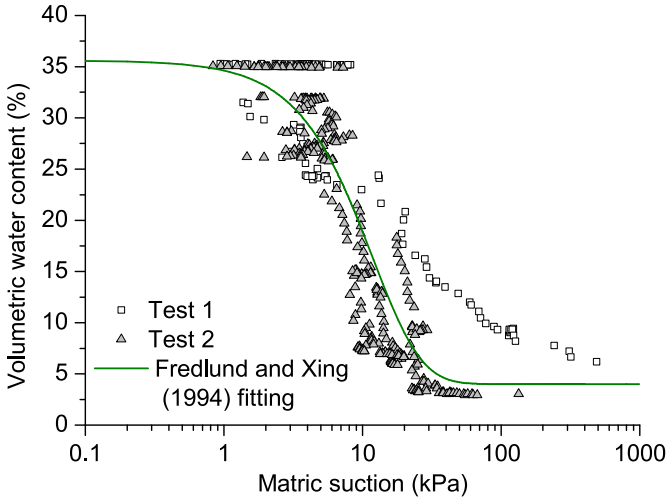

Fig. 5. Water retention curve determined using data of volumetric water content and suction from tests 1 and 2 (data from Song et al., 2014).

As mentioned previously through the observation of soil temperature variations (Fig. 2), during the evaporation process, the evaporative surface was going deeper. From the water retention curve, it was found that this evaporative surface corresponded to a suction of about 40 kPa. Thereby, it is possible to determine the dry layer depth d from the suction profile at a given time. In other words, Fig. 7 can be considered as representative of soil state at a given time.

By considering the relative humidity values at the soil surface $h_{\_surface}$ and at the evaporative surface $h_{\_drying}$, a function $f(d)$ can be defined:

$$f(d) = h_{\_drying} - h_{\_surface} \tag{7}$$

The $f(d)$ functions were determined for tests 1 and 2 using the experimental data and are shown in Table 1. A mean function $f(d)$ (test 1–2) was also determined considering both the results from tests 1 and 2.

The suction-related model proposed by Campbell (1985) and Wilson et al. (1997) has been widely used in describing the soil water evaporation rate as follows:

$$\frac{E_a}{E_p} = \frac{h_{\_surface} - h_a}{100 - h_a} \tag{8}$$

where h_a is the relative humidity of air (%); and E_p is the potential evaporation (mm/d), which corresponds to the case with water level at the soil surface.

Substituting Eq. (7) into Eq. (8) leads to

$$\frac{E_a}{E_p} = \frac{[h_{\_drying} - f(d)] - h_a}{100 - h_a} \tag{9}$$

The model proposed by Ta (2009) could be used to determine E_p:

$$E_p = (s_1 + s_2 u)(100 - h_a) \tag{10}$$

where u is the wind speed (m/s) at a reference elevation (taken equal to 50 mm above the soil (or water) surface); and s_1 and s_2 are the two constants whose values were determined through free water evaporation experiments under different atmospheric conditions, and $s_1 = 0.022$ and $s_2 = 0.031$ (see more details in Song et al., 2014).

Using Eqs. (9) and (10), the actual evaporation rate was calculated for tests 1 and 2. The calculated results were compared with the experimental ones in Fig. 6. A good agreement was obtained for both tests, showing the performance of the proposed model and the importance of considering the influence of the dry layer through $f(d)$ function. Note that the mean $f(d)$ function was used in the calculation.

2.3. Case of clay

To investigate the water evaporation mechanism for clayey soils, a test was performed on a clay taken from an embankment construction site in Héricourt, France. The clay was air-dried, ground and passed through 2 mm sieve. The soil sample was prepared by compaction using a manual compactor to reach a dry density of 1.4 Mg/m^3, which was also the dry density of soil used for the embankment construction in Héricourt (Dong, 2013). In order to ensure the soil homogeneity, the compaction was carried out in five layers of 50 mm thick each. The total thickness of the sample was thus 250 mm. More detail can be found in Song et al. (2016).

The actual evaporation rate determined is presented in Fig. 8. As for test 2 on sand (Fig. 6b), three zones were identified: a first zone with a constant value around 2.3 mm/d during the first 15 d, a second zone with a significant decrease to 0.5 mm/d at $t = 45$ d, and a third zone with a rate close to zero. The similar phenomenon was observed by Yanful and Choo (1997) on a clayey soil.

Unlike for sand, for the tested clay, significant cracking was observed. In order to quantitatively describe the cracking phenomenon, a surface crack ratio was adopted, which is the ratio of the surface of cracks to the total sample surface. The evolution of the surface crack ratio during the evaporation test is also shown in Fig. 8. Three zones were also observed: (i) a first zone with a slight increase until $t = 10$ d, (ii) a second zone with a rapid increase from $t = 10$ d to $t = 25.5$ d, and (iii) a third zone with a value around 25.3%. Comparison between the evolutions of actual evaporation rate and surface crack ratio showed that the initiation of cracking led to more water evaporation (the first zone). With further cracking, the evaporation rate was decreasing due to the less available water inside the soil (the second zone). Finally, when the soil water content became extremely low, the evolution of cracks reached a steady state and the evaporation rate approached zero. Further examination showed that the characteristic days separating different zones were not the same for the evaluations of surface crack ratio and actual evaporation, the evolution of actual evaporation curve lagging behind that of the surface crack ratio curve. This suggested that cracking was just one factor affecting the evaporation process, in addition to the factors related to soil conditions (suction and temperature) and atmospheric conditions (air relative humidity, air temperature, wind speed, etc.). To better appreciate the evolution of surface crack ratio, four photos of soil surface at different times are shown in Fig. 8.

As cracking can greatly affect the water evaporation for clays, it is of paramount importance to take it into account while developing evaporation models. Compared to the case of sand, the problem is more complex because the interface between the atmosphere and the soil is no longer horizontal – the interface becomes three-dimensional (3D) with complex water content distribution: the water content is expected to be higher in deeper level of cracks with larger distance to the soil surface or soil–atmosphere interface. Fig. 9 schematizes such evaporation configuration.

In Fig. 9, the 3D cracked surface of clay was assimilated to a horizontal atmosphere–soil interface by introducing two parameters: the surface crack ratio R_c and a relative humidity ratio $k = h_{\_crack}/h_{\_non\text{-}crack}$ where $h_{\_crack}$ is an equivalent relative

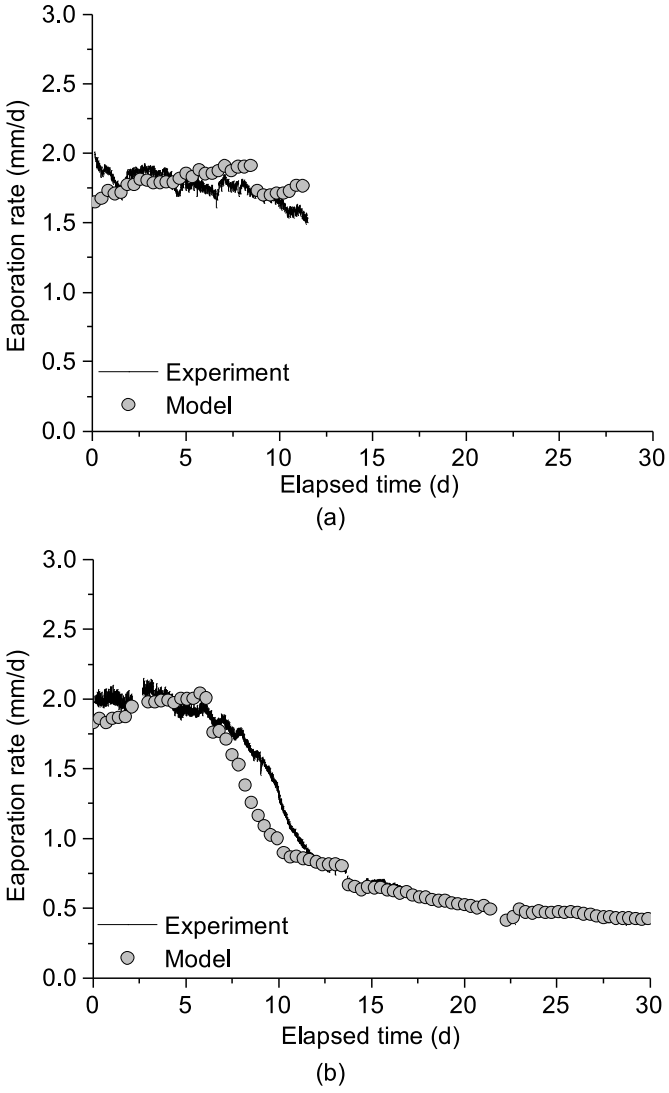

Fig. 6. Comparison of variations of evaporation rate between experiment and model: (a) Test 1 and (b) test 2 (data from Song et al., 2018).

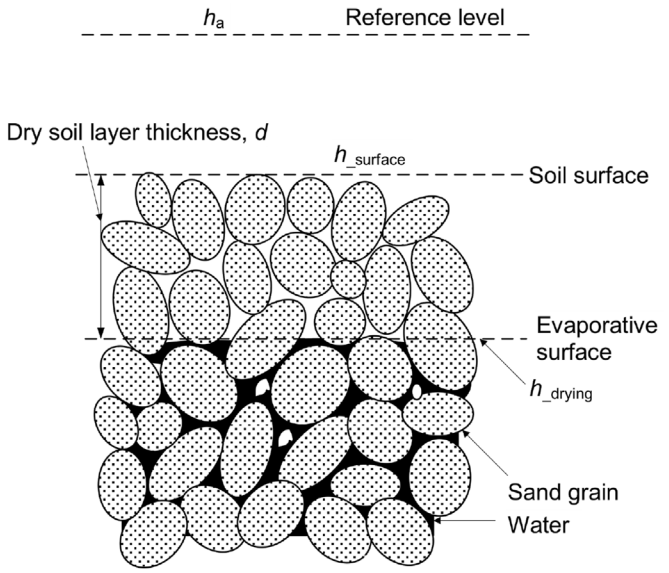

Fig. 7. Evaporation with a dry layer (modified from Song et al., 2018).

humidity inside the desiccation cracks and $h_{\_non\text{-}crack}$ is the relative humidity at the non-cracked surface. Normally, $h_{\_non\text{-}crack}$ is much lower than $h_{\_crack}$ because of the higher water content in cracks.

An equivalent relative humidity at the soil surface can then be defined as follows (Ta, 2009):

$$h_{\_surface} = R_c h_{\_crack} + (1 - R_c) h_{\_non-crack} \tag{11}$$

or

$$h_{\_surface} = [1 + (k - 1)R_c] h_{\_non-crack} \tag{12}$$

Substituting Eq. (12) into Eq. (8) leads to

$$\frac{E_a}{E_p} = \frac{[1 + (k - 1)R_c] h_{\_non-crack} - h_a}{100 - h_a} \tag{13}$$

Eq. (13) allows water evaporation to be calculated with consideration of the effect of cracks. Fig. 10 shows the comparison between the calculation and the measurement for the test conducted. A good agreement was obtained, showing the performance of the proposed model.

3. Field monitoring

Several studies were reported, aiming at investigating the soil–atmosphere interaction in field conditions (Cui et al., 2008; Bittelli et al., 2012; Smerthurst et al., 2012; Bicalho et al., 2018). It was found that it is the near surface zone that is affected the most by the climate changes. In this zone, the changes in temperature, water content and suction are the most significant, in agreement with the results obtained from the tests using environmental chamber (Figs. 2–4). As a result, the thermo-hydro-mechanical (THM) behavior of soil also changes significantly in this zone. In most cases, such climate effect has been accounted for in a simple way by considering the rainfall effect only (Cai and Ugai, 2004; Regmi et al., 2017). Bittelli et al. (2012) reported that using rainfall data only is not sufficient for assessing the landslide process, in particular for shallow clayey soils. It is thus necessary to consider the effects of full atmospheric conditions (solar radiation, air temperature, air relative humidity, wind speed, etc.) on the soil behavior (Hemmati et al., 2012; Cui et al., 2013; An et al., 2018b). In this regard, field monitoring with rich instrumentation of soil and rich measurements of air parameters is essential for further improving the analysis of the THM behavior of earth structures. In this section, an example of such field monitoring is given, involving an embankment constructed with lime/cement treated soils.

3.1. Embankment and instrumentation

Within an ANR (Agence Nationale de Recherche) project – TerDouest (ANR-07-PCGU-006-10), an experimental embankment was constructed at Héricourt, in the northeast of France where a continental climate dominates with oceanic influences. The embankment was 107 m long by 4.9 m high with side slopes of 1:2 (vertical: horizontal). The bottom was 25 m wide and the top was 5 m wide. The embankment was divided into two sections, constructed with a silty soil and a clayey soil, respectively. The silty soil

Table 1
Functions of $f(d)$ determined from tests 1 and 2.

Test	$f(d)$
1	$f(d) = 43.73 + (6.56–43.73)/\{1 + \exp[(d - 7.14)/1.24]\}$
2	$f(d) = 82.09 + (6.38–82.09)/\{1 + \exp[(d - 16.11)/1.69]\}$
1–2	$f(d) = 90.98 + (6.33–90.98)/\{1 + \exp[(d - 15.94)/2.85]\}$

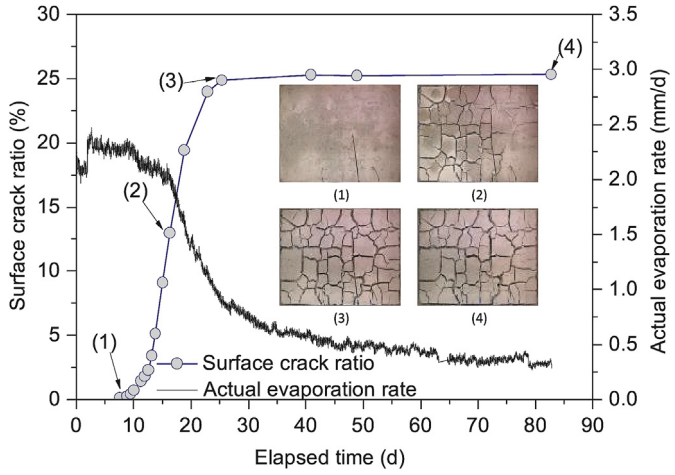

Fig. 8. Evolutions of actual evaporation rate and surface crack ratio (data from Song et al., 2016).

was classified as CL ($I_p = 18$), an inorganic clay with low plasticity, while the clayey soil as CH ($I_p = 45$), an inorganic clay with high plasticity. Both soils were treated with lime/cement in different dosages. The embankment consists of 17 layers with the two fill materials compacted at their standard optimum water contents. In total, 5280 m^3 of silty soil, 4710 m^3 of clayey soil, 320 t of lime and 162 t of cement were used.

The instrumentation layout was symmetrical for the two sections with the two treated fine-grained soils. Different sensors were installed in the embankment for monitoring the water content, suction, temperature and deformation in different positions. Four piezometers were installed to monitor the water table, two on the silty soil side and two on the clayey soil side. A system of runoff measurement was also installed to monitor the runoff from the side slope (An et al., 2017a). A meteorology station was installed on the top surface of embankment to record the meteorological data every 30 min, including solar radiation, precipitation, atmospheric pressure, wind speed and direction, air temperature and air relative humidity, at 0.5 m and 1.5 m above the top surface. In this section, only the soil suction and water content as well as the runoff are emphasized.

The Watermark soil suction sensors were used to monitor the matric suction. The working range of such sensor is 0–250 kPa. The reading frequency was once every 1–2 d. The time domain reflectometry (TDR) method was used to monitor the soil volumetric water content, together with the soil temperature. The reading frequency was every 3 h. More details can be found in Froumentin (2012).

3.2. Field monitoring data

Rich data were obtained from the field monitoring. However, for the purpose of illustrating the soil responses to the changes in meteorological conditions, only recordings of precipitation, volumetric water content, suction and runoff were presented here, as mentioned previously.

The variations of volumetric water content at points 1–4 are presented in Fig. 11, together with the precipitation, for the monitoring period from July 2010 to April 2014. Points 1 and 4 were situated 0.25 m far from the side slope; point 2 was situated 0.75 m far from the side slope; and point 3 was situated 2.4 m far from the side slope. Note that the same instrumentation was adopted for the silty soil and the clayey parts. In other words, there were the same positions 1–4 for the volumetric water content measurement in both parts. As the soils were treated with different binders (lime or cement) and with different dosages, for the purpose of comparison, only the points with the same treatment have been selected for analysis, as in Boussafir et al. (2018).

The case of silty soil treated with 2% lime is depicted in Fig. 11a. In terms of rainfall, relatively frequent and high intensity events occurred in the period from July 2010 to November 2011 and in the period from May to October 2012. Other periods seemed quite dry. Note, however, the extreme event in late March 2014 with an intensity as high as 19 mm (in 30 min). The variations of volumetric water content showed clearly that the further the point from the side surface, the smaller the variation – the variation at point 3 (2.4 m from the side slope) was much smaller than those at points 1 and 4. This indicated the significant effect of hydraulic conductivity on the water transfer inside the soil. The low permeability of the treated compacted silty soil (1×10^{-9} m/s) made the water transfer quite slow in the processes of infiltration during rainfalls and capillary movement during evaporation, limiting the variations of volumetric water content in the zone far from the side slope. Comparison between points 1 and 4 showed that the volumetric water content variation depended on elevation. Indeed, even though both points were situated at the same distance from the side slope (0.25 m), the variation at point 4 which had a lower elevation showed a higher mean value but lower fluctuation (or amplitude), suggesting a more intense influence of atmosphere in the higher elevation zone. This can be explained by the more contribution to the lower elevation zone by runoff during rainfalls and by capillary movement during evaporation. Two distinct decrease periods were observed at the two points, one from late March to early July 2011 and another from late May to early August 2013. Interestingly, in these two periods, there were no particularly less frequent and intensive rainfall events. This suggests a relatively significant water evaporation effect. Thereby, while analyzing the variation of water content inside a soil, considering the rainfalls only is not sufficient. It is of paramount importance to consider the full soil–atmosphere interaction. This was confirmed by the significant decrease of volumetric water content after the extreme event in late March 2014. Compared to the initial value (23.4%), the mean values of volumetric water content at all points significantly increased, suggesting that the monitoring period rather involved wet seasons.

The case of clayey soil treated with 4% lime is depicted in Fig. 11b, at points 1 and 2. The similar observation could be made: (i) the larger variation amplitude in the zone closer to the side slope (point 1), showing the more significant effect of atmospheric condition in the near surface zone; (ii) the higher mean volumetric water contents than the initial value (33.5%), indicating the wet monitoring period involved; and (iii) the lack of correspondence between the periods with significant decrease in volumetric water content and the dry period without rainfall events, showing the importance of considering both water infiltration and evaporation while assessing the variations of water content in soil.

Comparison between the case of silty soil (Fig. 11a) and the case of clayey soil (Fig. 11b) showed that the variation amplitudes are larger in the case of silty soil. This could be explained by the higher hydraulic conductivity of the silty soil. The mean values of volumetric water content of the silty soil were lower than those of clayey soil, suggesting a higher water retention capacity and a lower water evaporation for the clayey soil.

Fig. 12 shows the variations of suction at three different distances from the side surface (0.25 m, 0.5 m and 0.75 m), for the silty soil treated with 2% lime (Fig. 12a) and the clayey soil treated with 4% lime (Fig. 12b), in the period from July 2010 to October 2014 (8 months longer than that for the volumetric water content

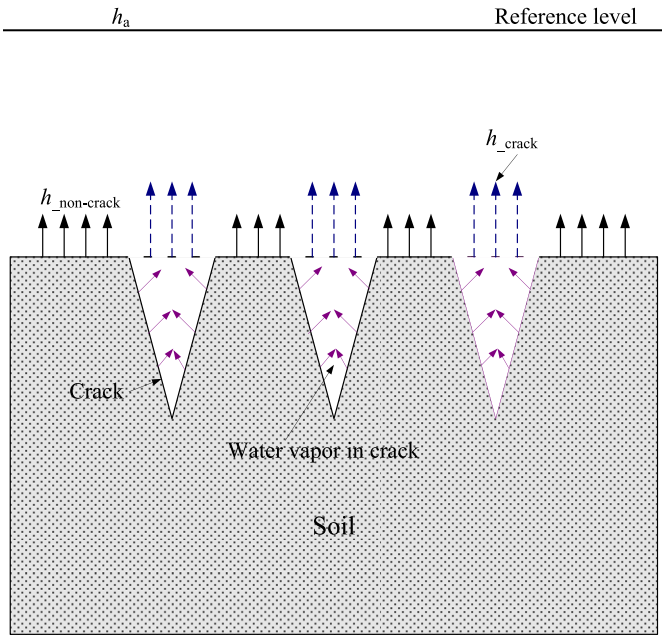

Fig. 9. Sketch of water evaporation from cracked clay (modified from Song and Cui, 2020).

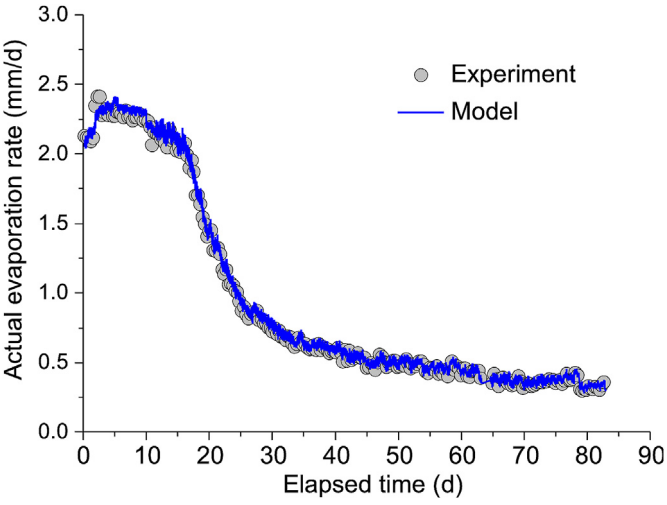

Fig. 10. Comparison between the measured and predicted actual evaporation rates.

recording). For the silty soil (Fig. 12a), four distinct high suction periods were observed: (i) from April to July 2011, (ii) in late February 2012, (iii) from June to September 2013, and (iv) from June to July 2014. By referring to the variations of volumetric water content (Fig. 11a), it appeared that the first and the third high suction periods coincided with the two periods with significant volumetric water content decreases. However, the second short high suction period did not seem to correspond to the volumetric water content variations. Further examination showed that this short high suction period only involved the measurement at the position 0.5 m far from the side slope, the suctions at the other two positions (0.25 m and 0.75 m) being much lower. It could thus be inferred that the high suction measured in this period at position 0.5 m might be related to a technical problem (likely of electronical nature) and should be ignored in further analysis. Because the fourth high suction period occurred without volumetric water content recordings, no correspondence could be attempted. In addition to these four distinct high suction periods, a number of lower suction periods could be identified, such as the period at the beginning of the recording (early July 2010) and the period from late July to early September 2012, which indicated the soil state with relatively higher water content (the suction peaks were relatively less pronounced).

For the clayey soil (Fig. 12b), six distinct high suction periods could be identified. The two low suction periods mentioned above for the silty soil became more distinct for the clayey soil, suggesting a higher sensitivity of clay to climate change than silt in terms of suction variation. The other four high suction periods corresponded to those identified on the silty soil. The suspected technical problem occurred also for the clayey soil, leading to the high suction period in late February 2012 with the recordings at position 0.25 m.

Comparison between the silty soil (Fig. 12a) and the clayey soil (Fig. 12b) showed that the variations of suction were more significant in the silty soil. This confirmed that the hydraulic conductivity is an important factor in the response of soil to the changes in atmospheric conditions – the silty soil had a higher hydraulic conductivity and its suction changed more under the effects of rainfall/evaporation.

During the rainfall events, the changes in soil water content or suction are governed by the quantity of water infiltrating into the soil. It is thus essential to determine the water infiltration based on the measured precipitation. For this purpose, it is necessary to have the measurements of runoff. Basically, surface runoff occurs when the rainfall rate exceeds the infiltration capacity of the soil (Beven, 2012). As direct measurement of runoff is difficult, indirect determination using correlations is often applied. One of the most widely used correlation is the Natural Resources Conservation Service (NRCS) runoff method (SCS, 1985), which allows runoff to be estimated from rainfall. Following this method, the measured runoff on the embankment slope is correlated with rainfall using the hourly recordings (mm/h), as shown in Fig. 13. It is interesting to note that the runoff remained quite low (<0.1 mm/h) when the precipitation was lower than about 11 mm/h, and became significant beyond 11 mm/h precipitation. Physically, the low runoff means that the water infiltration into the soil was dominating, while the significant runoff means that the runoff became dominant facing the water infiltration into the soil. Interestingly, a linear correlation was established between runoff and precipitation.

It is worth noting that the turning point at 11 mm/h precipitation is valid only for the embankment considered. When the geometry of embankment changes, this value is expected to be different.

4. Numerical modeling of soil–atmosphere interaction

The results obtained from the tests in the environmental chamber and from the field measurements showed the necessity of considering the full soil–atmosphere interaction in the assessment of soil suction and water content changes. In this section, such an approach is presented through modeling the soil responses to the changes in atmospheric conditions for the Héricourt embankment presented in the previous section. As the embankment was constructed with treated soils, the vertical deformation was found quite small (<0.3%). Thus, the volume change was not necessary to be accounted for, and only the coupled heat flow and water (liquid and vapor) flow needed to be taken into account. Note that when the volume change becomes a concern, a mechanical constitutive model needs to be incorporated (see for instance Hemmati et al., 2012; Cui et al., 2013).

The finite element method was adopted for the fully coupled thermo-hydraulic analysis. The boundary conditions at the soil–

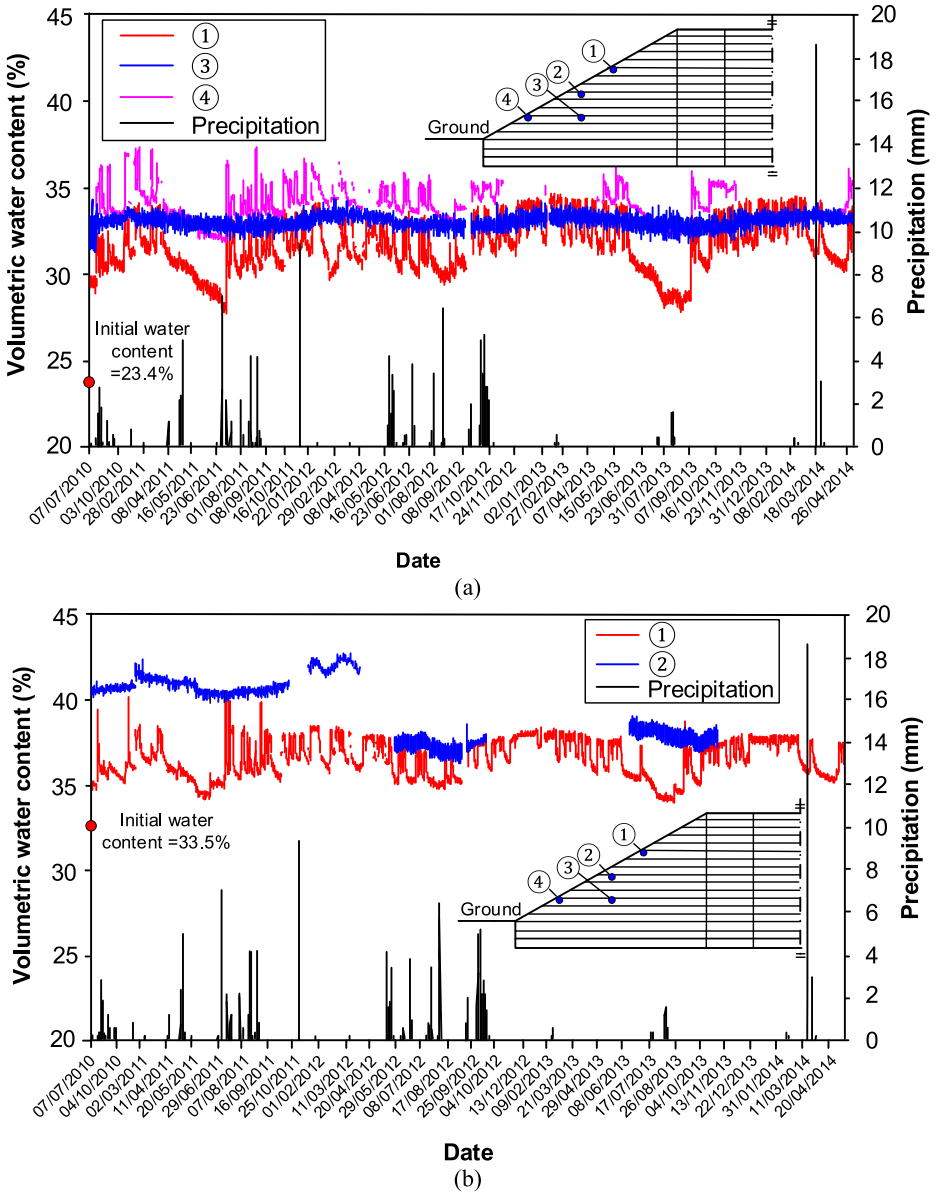

Fig. 11. Variations of volumetric water content and precipitation in the period from July 2010 to April 2014: (a) Silty soil with 2% lime and (b) clayey soil with 4% lime (data from Boussafir et al., 2018).

atmosphere interface were first determined using the water evaporation model as those presented in Section 1, based on the meteorological data and the initially estimated soil surface temperature and suction. Then, the numerical tool with implementation of the fully coupled thermo-hydraulic model was used for the calculation of soil temperature, water content and suction. The calculated temperature and soil suction on the boundary at the soil–atmosphere interface were used to define the new boundary condition for the next time step.

4.1. Soil–atmosphere interaction model

Two processes are involved in the soil–atmosphere interaction: water transfer and heat transfer. To determine the water transfer, the mass balance at the soil surface was used (without vegetation, see An et al., 2017b):

$$P = R_{\text{off}} + E_{\text{a}} + I_{\text{nf}} \tag{14}$$

where P is the precipitation (m/s), R_{off} is the runoff (m/s), and I_{nf} is the infiltration (m/s).

I_{nf} was used for defining the boundary condition in terms of water transfer. It can be positive (infiltration) or negative (evaporation). P and R_{off} were determined using direct field monitoring data. Eqs. (8) and (10) were used for the calculation of E_{a}.

To determine the heat transfer, the energy balance at the soil surface was used (An et al., 2017b):

$$R_{\text{n}} = G + L_{\text{E}} + H \tag{15}$$

where R_{n} is the net radiation flux (W/m^2), G is the soil heat flux (W/m^2), L_{E} is the latent heat flux (W/m^2), and H is the sensible heat flux (W/m^2).

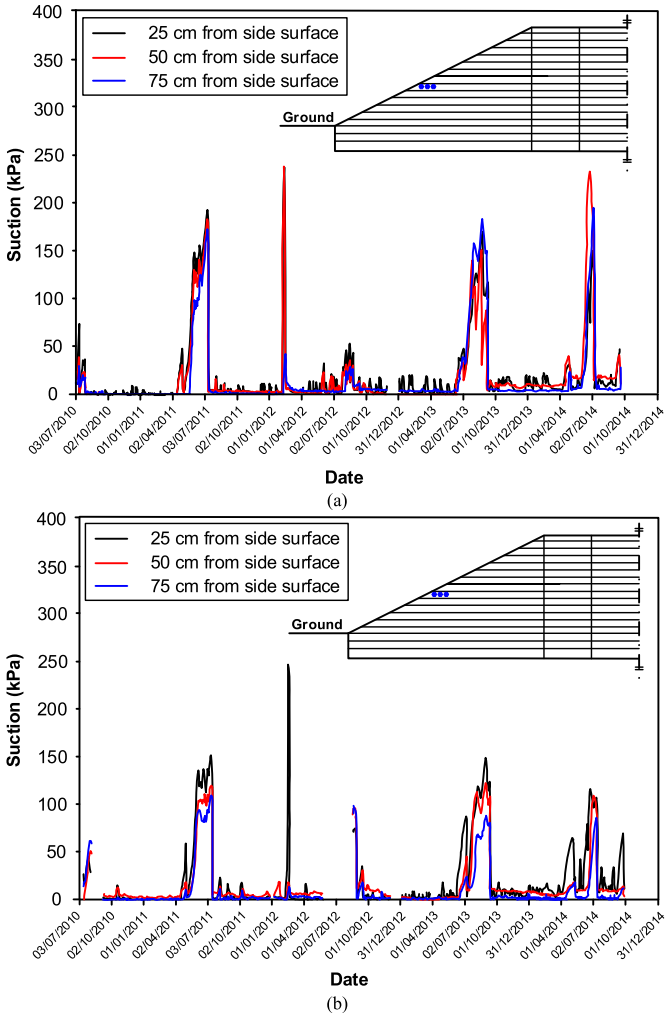

Fig. 12. Variations of suction in the period from July 2010 to October 2014: (a) Silty soil with 2% lime and (b) clayey soil with 4% lime (data from Boussafir et al., 2018).

G was used for defining the boundary condition in terms of heat transfer. It can be positive (soil heating) or negative (soil cooling). R_n was calculated from the measured total radiation flux using the expression proposed by Evett et al. (2011):

$$R_n = (1-\alpha)R_{si} - \left[a_c\left(\frac{R_{si}}{R_{so}}\right) + b_c\right]\left(a_1 + b_1 e_d^{0.5}\right)\sigma T_a^4 \tag{16}$$

where R_{si} is the solar irradiance at the surface (W/m^2); R_{so} is the solar radiation in the case of clear sky (W/m^2); σ is the Stefan–Boltzmann constant ($\sigma = 5.67 \times 10^{-8}$ W/(m^2 K^4)); a_c and b_c are the cloud factors ($a_c = 1.35$ and $b_c = -0.35$); a_1 and b_1 are the emissivity factors ($a_1 = 0.035$ and $b_1 = -0.14$); α is the soil surface albedo (α can be taken equal to 0.23 for the soils of Héricourt embankment); and e_d is the mean daily saturated vapor pressure, which was calculated from the mean daily dew point temperature T_d (°C) (Evett et al., 2011):

$$e_d = 0.611\exp\left(\frac{17.27T_d}{T_d + 237.3}\right) \tag{17}$$

In the case of clear sky, the solar radiation R_{so} (W/m^2) is calculated as (Evett et al., 2011):

$$R_{so} = (0.75 + 0.00002EL_{msl})R_{sa} \tag{18}$$

where EL_{msl} is the elevation above mean sea level (m), and R_{sa} is the extraterrestrial solar radiation (W/m^2) and was calculated by (Evett et al., 2011):

$$R_{sa} = \left[\frac{24(60)}{\pi}\right]G_{sc}d_r[\cos\phi\cos\delta(\sin w_2 - \sin w_1) + (w_2 - w_1)\sin\phi\sin\delta] \tag{19}$$

where G_{sc} is the solar constant (0.08202 MJ/(m^2 min)); d_r is the relative earth–sun distance; ϕ is the latitude (m); δ is the solar declination; w_1 and w_2 are the solar time angles (radian) at the beginning and end of the considered period, respectively, and were calculated by (Evett et al., 2011):

$$w_1 = w - \frac{\pi}{24/\tau} \tag{20}$$

$$w_2 = w + \frac{\pi}{24/\tau} \tag{21}$$

where w is the solar time angle (radian) at the center of the period, and τ is the length of the considered period (h).

The latent heat flux L_E (W/m^2) and sensible heat flux H (W/m^2) were respectively calculated by (Blight, 1997):

$$L_E = L_v E_a \tag{22}$$

$$H = \rho_a c_p K_H\left(\frac{\partial T_a}{\partial z}\right) \tag{23}$$

where L_v is the latent heat of water vaporization (J/kg), ρ_a is the air density (kg/m^3), c_p is the specific heat of air (J/(kg K)), K_H is the eddy diffusivity for heat through air (m^2/s), and z is the elevation (m).

4.2. Coupled thermo-hydraulic model

The mass transfer of water is the sum of liquid flow and vapor flow:

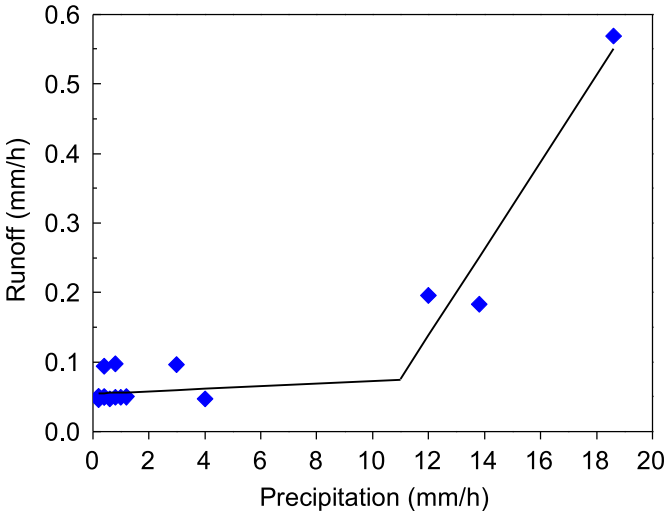

Fig. 13. Runoff measured on the side slope versus precipitation (data from An et al., 2017a).

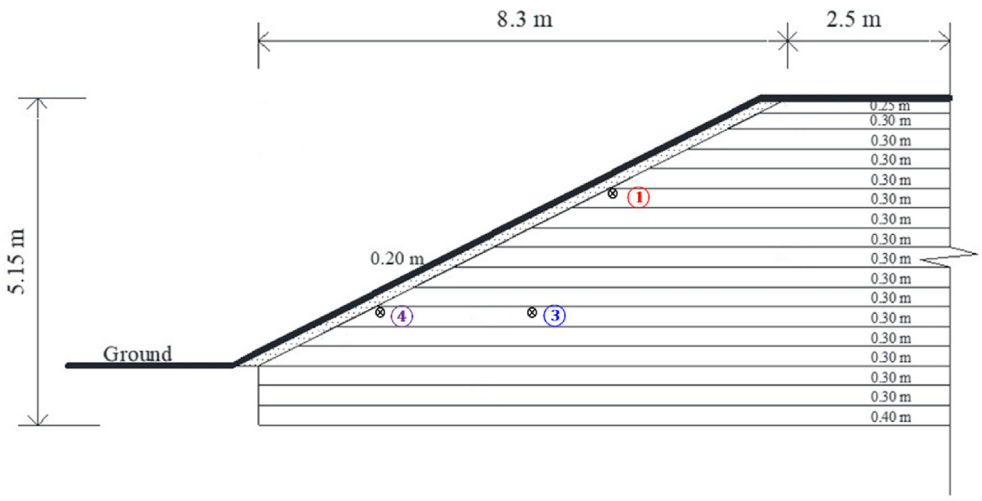

Fig. 14. Points considered in the numerical analysis (modified from An et al., 2017b).

$$\boldsymbol{q} = \boldsymbol{q}_{\mathrm{l}} + \boldsymbol{q}_{\mathrm{v}} \tag{24}$$

where $\boldsymbol{q}$ is the water flow density (kg/(s m^2)), $\boldsymbol{q}_{\mathrm{l}}$ is the liquid flow density (kg/(s m^2)), and $\boldsymbol{q}_{\mathrm{v}}$ is the vapor flow density (kg/(s m^2)). Darcy's law was used to describe the non-isothermal liquid flow:

$$\boldsymbol{q}_{\mathrm{l}} = -K\rho_{\mathrm{l}}\nabla(\varphi + z) \tag{25}$$

where K is the unsaturated hydraulic conductivity (m/s), and φ is the hydraulic head (m).

Fick's law was used to describe the vapor flow by diffusion (Philip and De Vries, 1957):

$$\boldsymbol{q}_{\mathrm{v}} = -D_{\mathrm{atm}}\varepsilon\beta\nabla\rho_{\mathrm{v}} \tag{26}$$

where D_{atm} is the molecular diffusivity of vapor in the air (m^2/s), ε is the tortuosity of soil, β is the cross-sectional area of soil, and ρ_{v} is the density of vapor (kg/m^3) calculated by Philip and De Vries (1957):

$$\rho_{\mathrm{v}} = \rho_0 \exp[\varphi g M_{\mathrm{w}} / (RT)] \tag{27}$$

where ρ_0 is the density of saturated water vapor (kg/m^3), g is the gravitational acceleration (m/s^2), M_{w} is the molar mass of water molecule (kg/mol), and T is the absolute temperature (K).

Fourier's law was used to describe the transferred heat flux through soil–atmosphere interface $\boldsymbol{Q}$ (W/m^2):

$$\boldsymbol{Q} = -\lambda\nabla T + L_{\mathrm{v}}\boldsymbol{q}_{\mathrm{v}} \tag{28}$$

where λ is the soil thermal conductivity (W/(m K)).

By substituting the fundamental equations (Eqs. (24) and (28)) into the conservation equations for water and heat, respectively, the governing equations can be obtained. More details can be found in An et al. (2017b).

4.3. Simulating the thermo-hydraulic responses of Héricourt embankment

The proposed thermo-hydraulic model was implemented in the FreeFem++ code (Hecht, 2012) for analyzing the thermo-hydraulic behavior of Héricourt embankment. Examination of all data in the monitoring period showed that only the recordings during July 6–26, 2011, are regular and complete. Thus, this short period was selected for the numerical analysis. The soil temperature and volumetric water content values on July 6, 2011 at 14:42:52 were taken to define the initial conditions. The meteorological data were used to determine the infiltration (positive or negative) and the soil heat flux (positive or negative) using the soil–atmosphere interaction model. The obtained values were used to define the boundary conditions at the soil–atmosphere interface. A water table depth of 5 m below the ground surface was considered, where the soil suction was taken equal to zero. As only the temperature at the base of the embankment was available, this temperature was used to define the thermal bottom boundary condition by assuming that the temperature changed a little from the base of the embankment to the water table.

The silty soil part of the embankment was selected for the analysis. For simplicity, this part of embankment was considered as homogeneous. As proposed by De Vries (1963) and Cui et al. (2005), the soil thermal conductivity λ (W/(m K)) was assumed to vary linearly with the volumetric water content θ_{w}:

$$\lambda = 2.1818\theta_{\mathrm{w}} + 0.808 \tag{29}$$

The soil water retention curve was determined in the laboratory using soil samples taken from the Héricourt site. van Genuchten (1980)'s model was used to fit the curve:

$$S_{\mathrm{e}} = \frac{\theta_{\mathrm{w}} - \theta_{\mathrm{r}}}{\theta_{\mathrm{s}} - \theta_{\mathrm{r}}} = \left[\frac{1}{1 + (a\varphi)^n}\right]^m \tag{30}$$

where S_{e} is the effective degree of saturation; θ_{s} is the saturated volumetric water content ($\theta_{\mathrm{s}} = 0.4$); θ_{r} is the residual volumetric water content ($\theta_{\mathrm{r}} = 0.004$); and a, m and n are the fitting parameters ($a = 0.003$ kPa^{-1}, $m = 0.18$, and $n = 1.8$).

The hydraulic conductivity was also estimated from van Genuchten (1980)'s model:

$$K = K_{\mathrm{s}} S_{\mathrm{e}}^{0.5}\left[1 - \left(1 - S_{\mathrm{e}}^{1/m_1}\right)^{m_1}\right]^2 \tag{31}$$

where K_{s} is the soil saturated hydraulic conductivity ($K_{\mathrm{s}} = 1 \times 10^{-9}$ m/s according to the laboratory measurement), and m_1 is a fitting parameter ($m_1 = 0.5$).

The three monitoring points 1, 3 and 4 presented in Fig. 11a were considered. As a cover layer of about 0.2 m was put on the side slope

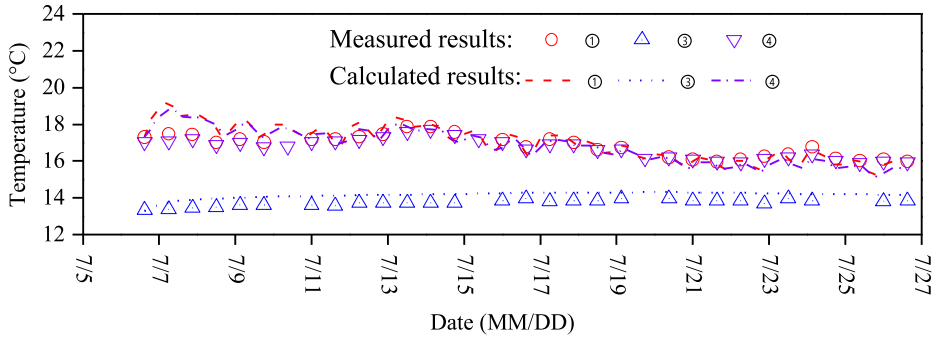

Fig. 15. Comparison of temperature changes between calculation and measurement in July 2011 (data from An et al., 2017b).

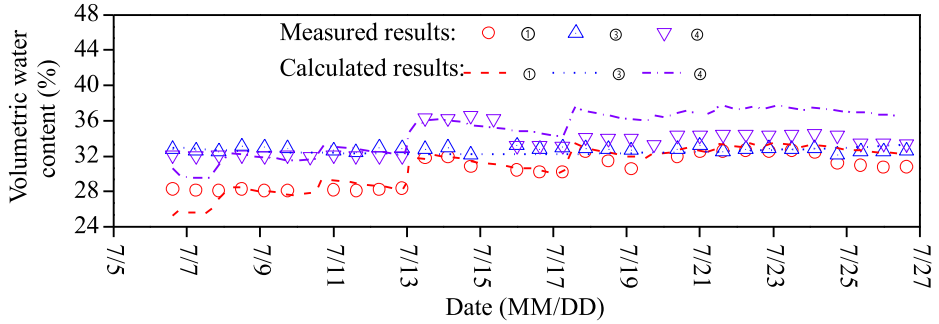

Fig. 16. Comparison of changes in volumetric water content between calculation and measurement in July 2011 (data from An et al., 2017b).

after the construction of the core part of embankment by compaction, this layer was considered in the numerical analysis (Fig. 14). It was assumed that this layer was homogeneous. As it was not compacted, a relatively lower thermal conductivity of 0.25 W/(m K) and a relatively higher hydraulic conductivity of 1×10^{-8} m/s were considered.

As regular recordings of every 3 h were performed for soil temperature and volumetric water content, while one value was recorded every 1–2 d for the soil suction, in order to well reveal the variations of soil thermo-hydraulic response during day and night times, only the soil temperature and volumetric water content were selected for the comparative analysis.

Fig. 15 shows the comparisons of the variations of temperature between calculation and measurement at points 1, 3 and 4. For clarity, a number of skip points equal to 5 were adopted for representing the measured results. Note that for some periods, the data were not available. It appeared that the proposed numerical approach allowed the soil temperature to be reasonably well predicted, even though a slightly higher temperature was calculated for points 1 and 4 in the first 2 d. Moreover, the measurement showed that the temperature at point 1 was slightly higher than that at point 4, and this was well reproduced by the numerical calculation. Note that the lower temperature at point 3 was due to its further distance from the side slope. The slightly higher temperature at point 1 than at point 4 was to be related to the slower water evaporation at point 1. Indeed, as the volumetric water content was lower at point 1 (see Fig. 11a), the corresponding suction must be higher. Thus, the water evaporation rate must be slower, as described in the first section.

Fig. 16 shows the comparisons of the variations of volumetric water content between calculation and measurement. Again, for clarity, a number of skip points equal to 5 were adopted for representing the available measured results. For point 1, an overall good agreement was obtained except the beginning where a slightly lower value was predicted and the end where a slightly higher value was predicted. For point 3, the variation was small during the whole period and the calculation agreed well with the measurement. For point 4, slightly lower values were given by the calculation for the first 2 d and slightly higher values were predicted for the period from July 18 to the end. On the whole, all variations of volumetric water content were reasonably well predicted.

5. Conclusions

Facing the global warming, the effect of climate change on the earth structures has become an increasing concern in the community of geotechnical engineering. To address this concern, it appeared important to better understand the fundamental mechanisms involved in water evaporation process for different soils by performing laboratory tests, to upscale the laboratory condition to the field condition by performing field monitoring, and to develop numerical tools for analyzing and predicting the long-term behavior of earth structures by considering the soil–atmosphere interaction. This paper aims at illustrating such methodology through some representative studies.

For bare soils, the water evaporation process is governed by the atmospheric conditions and soil hydraulic conditions. Evaporation is enhanced by low air relative humidity, high air temperature, high wind speed, and low soil suction or high water content. This evaporation process can be well described by suction-related models such as the model proposed by Campbell (1985) and Wilson et al. (1997). However, depending on the soil involved, different physical phenomena should be taken into account. For sandy soils, as their water retention capacity is relatively low and a suction lower than 100 kPa may make them dry, the evaporative surface is not constantly at the ground surface – it becomes deeper and deeper upon drying. In that case, liquid water transfer by

capillary effect in the soil below the evaporative surface and vapor transfer by diffusion in the dry layer above the evaporative surface should be accounted for while analyzing the evaporation process. This can be done by incorporating a function representing the difference of relative humidity between the evaporative surface and the ground surface into the suction-related models. For clayey soils, cracks occur in general upon drying. This changes the one-dimensional (1D) evaporation problem to a 3D problem – the evaporative surface is no longer horizontal because cracks are involved with varying water content in them. To account for the effect of cracks in the evaporation process, two parameters can be introduced: a surface crack ratio which represents the ratio of crack surface to the total surface, and a relative humidity ratio which represents the ratio of equivalent relative humidity of cracks to the humidity of the non-cracked part. Comparisons between the models and measurements showed the relevance of such approaches.

The instrumentation for field monitoring should cover both the soil and the atmosphere, with emphasis put on the near surface zone of soil where the soil–atmosphere interaction is expected to be the most significant. The common method of considering weather effect on soil behavior is to account for the precipitation effect. The field data showed that for a slope like the side slope of an embankment, this is far from being satisfactory. First, it is important to consider the runoff in the estimation of water infiltration when the rainfall is higher than a threshold value (about 11 mm/h for the Héricourt embankment). Second, there is no always a satisfactory correlation between the precipitation and soil water content change or soil suction change because of the effect of runoff and the water movement inside the soil under the effect of suction. In the zone far from the soil surface, the changes in water content or suction are small, indicating a limited effect of atmosphere. In the zone near the soil surface, the climate effect is significant. On the side slope of embankment, the positions with higher elevations have a lower water content, higher suction and higher temperature. The lower water content and higher suction can be explained by the contributions of runoff and the water movement inside the soil by capillary effect, while the higher temperature can be explained by the lower evaporation due to the higher suction. Comparison between the silty soil and the clayey soil showed that the variations of water content and suction are smaller in the clayey soil, suggesting the importance of the soil hydraulic conductivity in soil–atmosphere interaction – the higher the hydraulic conductivity, the more significant the soil–atmosphere interaction.

By considering the water (liquid and vapor) flows and the heat flow in a coupled thermo-hydraulic model for the soil and a suction-related soil–atmosphere interaction model for the soil-atmosphere interface, the soil thermo-hydraulic behavior can be well described. Indeed, comparison between calculations and measurements showed that such a numerical approach can well predict the variations of soil temperature, water content and suction using the meteorological data, in particular the smaller variations in the zone far from the soil–atmosphere interface, the higher temperature and lower water content at higher elevations on the side slope of embankment. It is worth noting that the developed numerical approach was successfully applied in analyzing another embankment constructed with lime-treated silty soil (An et al., 2018b) and in evaluating the long-term thermo-hydraulic behavior of a future site for the disposal of short-lived low and intermediate level nuclear waste (An et al., 2020). Nevertheless, it should be mentioned that in the analyzed embankment case, no retained water was considered. The presence of retained water can greatly change the water content and suction of soil, thus the soil–atmosphere interaction. Moreover, as the analyzed embankment was not quite high (4.9 m), it was not necessary to distinguish the sunny and non-sunny slope sides. In case of much higher embankment, the solar radiation can be significantly different for the two kinds of slope sides, and the consideration of such difference in the numerical analysis becomes necessary.

It is also worth noting that this paper did not address the effect of vegetation which is an important issue to deal with while investigating the climate effect on earth structures. The vegetation can not only greatly affect the soil water evaporation through interception and transpiration, but also modify the soil THM behavior through the development of root architecture. Furthermore, the volume change behavior was not accounted for in the numerical analysis because of the negligible vertical deformation recorded for the studied embankment with treated soils. In some cases, this mechanical aspect can be important, in particular for clayey soils. To incorporate such mechanical aspect, it is necessary to use a fully coupled THM model for soils (see for instance Hemmati et al., 2012), together with a soil–atmosphere interaction model for the soil–atmosphere interface.

Declaration of competing interest

The authors declare that they have no known competing financial interests or personal relationships that could have appeared to influence the work reported in this paper.

Acknowledgments

The support from the French Research Agency (ANR) within the Project TerDOUEST ANR-07-PCGU-006-10 is greatly acknowledged. The author is also grateful to Dr Weikang Song, Dr Ni An and Dr Zi Ying for their help in improving the illustrations.

Notation

A	Area of the evaporative surface (m^2)
a, m, n	Fitting parameters for soil water retention curves
a_1	Emissivity factor (0.035)
a_c	Cloud factor (1.35)
b_1	Emissivity factor (−0.14)
b_c	Cloud factor (−0.35)
c_p	Specific heat of air (J/(kg K))
d	Dry layer depth (m)
D_{atm}	Molecular diffusivity of vapor in the air (m^2/s)
e	Base of natural logarithm
e_a	Vapor pressure (Pa)
e_d	Mean daily saturated vapor pressure (Pa)
e_{sat}	Saturated vapor pressure (Pa)
E_a	Actual evaporation rate (mm/d or m/s)
E_p	Potential evaporation rate (mm/d)
EL_{msl}	Elevation above mean sea level (m)
g	Gravitational acceleration (m/s^2)
G	Soil heat flux (W/m^2)
H	Sensible heat flux(W/m^2)
H_a	Absolute humidity (Mg/m^3)
H_r	Air relative humidity (%)
$H_{a\text{-outlet}}$	Absolute humidity at the outlet of the chamber (Mg/m^3)
$H_{a\text{-inlet}}$	Absolute humidity at the inlet of the chamber (Mg/m^3)
h_a	Relative humidity value of air (%)
$h_{\_crack}$	Equivalent relative humidity inside the desiccation cracks (%)
$h_{\_non\text{-}crack}$	Relative humidity at the non-cracked surface (%)
$h_{\_surface}$	Relative humidity value at the soil surface (%)
$h_{\_drying}$	Relative humidity value at the evaporative surface (%)
I_{nf}	Infiltration (m/s)
k	Relative humidity ratio $h_{\_crack}/h_{\_non-crack}$

K	Unsaturated hydraulic conductivity (m/s)
K_H	Eddy diffusivity for heat through air (m^2/s)
K_s	Saturated hydraulic conductivity (m/s)
L_E	Latent heat flux (W/m^2)
L_v	Latent heat of water vaporization (J/kg)
M_w	Molar mass of water molecule (kg/mol)
m_1	Fitting parameter
P	Precipitation (m/s)
$\boldsymbol{q}$	Water flow desnity (kg/(s m^2))
$\boldsymbol{q}_l$	Liquid flow desnity (kg/(s m^2))
$\boldsymbol{q}_v$	Vapor flow desnity (kg/(s m^2))
$\boldsymbol{Q}$	Transferred heat flux through soil–atmosphere interface (W/m^2)
Q_a	Air flow rate through the chamber (L/s)
R	Gas constant (J/(kg K) or J/(mol K))
R_c	Surface crack ratio
R_n	Net radiation flux (W/m^2)
R_{off}	Runoff (m/s)
R_{si}	Solar irradiance at the surface (W/m^2)
R_{sa}	Extraterrestrial solar radiation (W/m^2)
R_{so}	Solar radiation in the case of clear sky (W/m2)
S_e	Effective degree of saturation
s_1, s_2	Empirical constants
T	Absolute temperature (K)
T_a	Air temperature (K or °C)
T_d	Mean daily dew point temperature (°C)
u	Wind speed at a reference elevation (m/s)
w	Solar time angle at the center of the considered period (radian)
w_1	Solar time angle at the beginning of the considered period (radian)
w_2	Solar time angle at the end of the considered period (radian)
z	Elevation (m)
α	Soil surface albedo (0.23)
β	Cross-sectional area of soil
δ	Solar declination
ε	Tortuosity of soil
θ_r	Residual volumetric water content (%)
θ_s	Volumetric water content in saturated state (%)
θ_w	Volumetric water content (%)
λ	Soil thermal conductivity (W/(m K))
ρ_0	Density of saturated water vapor (kg/m^3)
ρ_a	Density of air (kg/m^3)
ρ_v	Density of vapor (kg/m^3)
ρ_l	Density of liquid (Mg/m^3 or kg/m^3)
σ	Stefan–Boltzmann constant (5.67×10^{-8} W/(m^2 K^4))
τ	Length of the considered period (h)
φ	Hydraulic head (m)
ψ	Matric suction (kPa)
ϕ	Latitude (m)
G_{sc}	Solar constant
d_r	Relative earth–sun distance

References

Allman, M.A., Delaney, M.D., Smith, D.W., 1998. A field study of seasonal ground movement in expansive soils. In: Proceedings of the 2nd International Conference on Unsaturated Soils (UNSAT'98). International Academic Publishing House, Beijing, China, pp. 309–314.

Aluwihare, S., Watanabe, K., 2003. Measurement of evaporation on bare soil and estimating surface resistance. J. Environ. Eng. 129 (12), 1157–1168.

An, N., Hemmati, S., Cui, Y.J., Mercadier, D., 2017a. Assessment of rainfall runoff based on the field measurement on an embankment. Geotech. Test J. 40 (1), 29–36.

An, N., Hemmati, S., Cui, Y.J., 2017b. Numerical analysis of soil volumetric water content and temperature variations in an embankment due to soil-atmosphere interaction. Comput. Geotech. 83, 40–51.

An, N., Tang, C.S., Xu, S.K., Gong, X.P., Shi, B., Inyang, H.I., 2018a. Effects of soil characteristics on moisture evaporation. Eng. Geol. 239, 126–135.

An, N., Hemmati, S., Cui, Y.J., Maisonnave, C., Charles, I., Tang, C.S., 2018b. Numerical analysis of hydro-thermal behaviour of Rouen embankment under climate effect. Comput. Geotech. 99, 137–148.

An, N., Cui, Y.J., Conil, N., Talandier, J., Conil, S., 2020. Soil–atmosphere interaction in the verburden of a short-lived low and intermediate level nuclear waste (LLW/ILW) disposal facility. Comput. Geotech. 124, 103610.

Beven, K., 2012. Rainfall-runoff Modeling: the Primer, second ed. Lancanster University, Lancanster, UK.

Bittelli, M., Valentino, R., Salvatorelli, F., Pisa, P.R., 2012. Monitoring soil-water and displacement conditions leading to landslide occurrence in partially saturated clays. Geomorphology 173–174, 161–173.

Bicalho, K., Boussafir, Y., Cui, Y.J., 2018. Performance of an instrumented embankment constructed with lime-treated silty clay during four-years in the North-east of France. Transp. Geotech. 17, 100–116.

Biddle, P.G., 1983. Patterns of soil drying and moisture deficit in the vicinity of trees on clay soils. Geotechnique 33 (2), 107–126.

Blight, G.E., 1997. Interactions between the atmosphere and the earth. Geotechnique 47 (4), 715–767.

Boussafir, Y., Bicalho, K., Cui, Y.J., Mercadier, D., 2018. Vers une meilleure compréhension des interactions sol-atmosphère d'un remblai grâce au monitoring. In: Proceedings of Neuvième Journées Nationales de Géotechnique et de Géologie de l'Ingénieur, Marne-la-Vallée, France (in French).

Brutsaert, W., 1988. Evaporation into the Atmosphere: Theory, History, and Applications. D. Reidel Publishing Company, Dordrecht, Netherlands.

Campbell, G.S., 1985. Soil Physics with Basic: Transport Models for Soil-Plant Systems. Elsevier, Amsterdam, Oxford.

Cai, F., Ugai, K., 2004. Numerical analysis of rainfall effects on slope stability. Int. J. GeoMech. 4 (2), 69–78.

Chang, K.T., Lee, K.Z.Z., Wu, H.Y., 2020. Internal erosion failure of uniform sands under confinement and constricted seepage exit. Water 12 (9), 2417.

Cui, Y.J., Lu, Y.F., Delage, P., Riffard, M., 2005. Field simulation of in-situ water content and temperature changes due to ground-atmospheric conditions. Geotechnique 55 (7), 557–567.

Cui, Y.J., Tang, A.M., Mantho, A., De Laure, E., 2008. Monitoring field soil suction using miniature tensiometer. Geotech. Test J. 31 (1), 95–100.

Cui, Y.J., Zornberg, J.G., 2008. Water balance and evapotranspiration monitoring in geotechnical and geoenvironmental engineering. Geotech. Geol. Eng. 26 (6), 783–798.

Cui, Y.J., Ta, A.N., Hemmati, S., Tang, A.M., Gatmiri, B., 2013. Experimental and numerical investigation of soil-atmosphere interaction. Eng. Geol. 165, 20–28.

De Vries, D.A., 1963. Thermal properties of soils. In: Van Wijk, W.R. (Ed.), Physics of Plant Environment. North-Holland, Amsterdam, Netherlands, pp. 210–235.

Dong, J.C., 2013. Investigation of Aggregates Size Effect on the Stiffness of Lime And/or Cement Treated Soil: from Laboratory to Field Conditions. PhD Thesis. Université Paris-Est, Paris, France.

Driscoll, R., 1983. The influence of vegetation on the swelling and shrinking of clay soils in Britain. Geotechnique 33 (2), 93–105.

Evett, S.R., Prueger, J.H., Tolk, J.A., 2011. Water and energy balances in the soil-plant-atmosphere continuum. In: Huang, P.M., Li, Y.C., Sumner, M.E. (Eds.), Y. Handbook of Soil Sciences: Properties and Processes, second ed. CRC Press, Boca Raton, Florida, USA, pp. 6-1–6-44.

Fredlund, D.G., Xing, A., 1994. Equations for the soil-water characteristic curve. Can. Geotech. J. 31 (4), 521–532.

Froumentin, M., 2012. Rapport de construction de l'ouvrage expérimental RD438 Héricourt (70). Project TerDOUEST – ANR-07-PCGU-006-10 (in French).

Gao, D.Z., 1995. The cause of a large number of houses damage. In: Proceedings of the 1st International Conference on Unsaturated Soils (UNSAT'95). A.A. Balkema, Rotterdam, Netherlands, pp. 863–867.

Hecht, F., 2012. New development in FreeFem++. J. Numer. Math. 20 (3–4), 251–265.

Hemmati, S., Gatmiri, B., Cui, Y.J., Vincent, M., 2012. Thermo-hydro-mechanical modelling of soil settlements induced by soil-vegetation-atmosphere interactions. Eng. Geol. 139–140, 1–16.

Holtz, W.G., 1983. The influence of vegetation on the swelling and shrinking of clays in the United States of America. Geotechnique 33 (2), 159–163.

IPCC, 2014. Climate Change 2014 Synthesis Report. Contribution of Working Groups I, II and III to the Fifth Assessment Report of the Intergovernmental Panel on Climate Change (IPCC). IPCC, Geneva, Switzerland.

IPCC, 2018. Global Warming of 1.5 °C. An IPCC Special Report on the Impacts of Global Warming of 1.5 °C above Pre-industrial Levels and Related Global Greenhouse Gas Emission Pathways, in the Context of Strengthening the Global Response to the Threat of Climate Change, Sustainable Development, and Efforts to Eradicate Poverty. IPCC, Geneva, Switzerland (in press). https://www.ipcc.ch/site/assets/uploads/sites/2/2019/06/SR15_Full_Report_High_Res.pdf.

Nahlawi, H., Kodikara, J., 2006. Laboratory experiments on desiccation cracking of thin soil layers. Geotech. Geol. Eng. 24 (6), 1641–1664.

Philip, J.R., De Vries, D.A., 1957. Moisture movement in porous materials under temperature gradients. Eos Trans. Am Geophys. Union 38 (2), 222–232.

Ravina, I., 1983. The influence of vegetation on moisture and volume changes. Geotechnique 33 (2), 151–163.

Regmi, R.K., Jung, K., Nakagawa, H., Do, X.K., Mishra, B.K., 2017. Numerical analysis of multiple slope failure due to rainfall: based on laboratory experiments. Catena 150, 173–191.
SCS, 1985. National Engineering Handbook, Section 4: Hydrology. USDA Soil Conservation Service, Washington, D.C., USA.
Smerthurst, J.A., Clarke, D., Powrie, W., 2012. Factors controlling the seasonal variation in soil water content and pore water pressures within a lightly vegetated clay slope. Geotechnique 62 (5), 429–446.
Song, W.K., Cui, Y.J., Tang, A.M., Ding, W.Q., 2013. Development of a large-scale environmental chamber for investigating soil water evaporation. Geotech. Test J. 36 (6), 847–857.
Song, W.K., Cui, Y.J., Tang, A.M., Ding, W.Q., Tran, T.D., 2014. Experimental study on water evaporation from sand using environmental chamber. Can. Geotech. J. 51 (2), 115–128.
Song, W.K., Cui, Y.J., Tang, A.M., Ding, W.Q., Wang, Q., 2016. Experimental study on water evaporation from compacted clay using environmental chamber. Can. Geotech. J. 53 (8), 1293–1304.
Song, W.K., Cui, Y.J., Ye, W.M., 2018. Modelling of water evaporation from bare sand. Eng. Geol. 233, 281–289.
Song, W.K., Cui, Y.J., 2020. Modelling of water evaporation from cracked clayey soil. Eng. Geol. 266, 105465.
Ta, A.N., 2009. Etude de l'interaction sol-atmosphere en chambre environmentale. PhD Thesis. Ecole des Ponts ParisTech, Paris, France (in French).
Tang, A.M., Ta, A.N., Cui, Y.J., Thiriat, J., 2009. Development of a large scale infiltration tank for determination of the hydraulic properties of expansive clays. Geotech. Test J. 32 (5), 385–396.
Tang, C.S., Cui, Y.J., Tang, A.M., Shi, B., 2010. Experiment evidence on the temperature dependence of desiccation cracking behavior of clayey soils. Eng. Geol. 114 (3–4), 261–266.
Tang, C.S., Shi, B., Liu, C., Gao, L., Inyang, H.I., 2011. Experimental investigation of the desiccation cracking behavior of soil layers during drying. J. Mater. Civ. Eng. 23 (6), 873–878.
Vandangeon, P., 1992. Exemple de sinistres en région parisienne. Rev. Fr. Geotech. 58, 7–14 (in French).
van Genuchten, M.T., 1980. A closed-form equation for predicting the hydraulic conductivity of unsaturated. Soil Sci. Soc. Am. J. 44 (5), 892–898.
Williams, A.A.B., Pidgeon, J.T., 1983. Evapo-transpiration and heaving clays in South Africa. Geotechnique 33 (2), 141–150.
Wilson, G.W., Fredlund, D.G., Barbour, S.L., 1994. Coupled soil-atmosphere modelling for soil evaporation. Can. Geotech. J. 31 (2), 151–161.
Wilson, G.W., Fredlund, D.G., Barbour, S.L., 1997. The effect of soil suction on evaporative fluxes from soil surfaces. Can. Geotech. J. 34 (1), 145–155.
Yanful, E.K., Choo, L.P., 1997. Measurement of evaporative fluxes from candidate cover soils. Can. Geotech. J. 34 (3), 447–459.
Yanful, E.K., Mousavi, S.M., Yang, M., 2003. Modeling and measurement of evaporation in moisture-retaining soil covers. Adv. Environ. Res. 7 (4), 783–801.
Yesiller, N., Miller, C.J., Inci, G., Yaldo, K., 2000. Desiccation and cracking behavior of three compacted landfill liner soils. Eng. Geol. 57 (1–2), 105–121.

Yu-Jun Cui obtained his BSc degree in Civil Engineering from Tongji University, China, in 1984, his Master degree in Mechanics applied to Constructions from Ecole des Ponts ParisTech (ENPC), France, in 1989 and his PhD in Unsaturated Soil Mechanics in 1993, also from Ecole des Ponts ParisTech (ENPC). He was employed by ENPC immediately after his PhD as an assistant researcher in the Laboratory of Soil Mechanics (CERMES) now becoming Géotechnique Group of Laboratoire Navier. He passed his Habilitation to Direct Research in Civil Engineering at University of Marne La Vallée, France, in 2000, and obtained the position of professor of ENPC in 2005. He has been Head of Master MSROE (Mécanique des Sols, des Roches et des Ouvrages dans leur Environnement) since 2004. His research interests cover unsaturated soil mechanics, laboratory testing, constitutive modelling, environmental geotechnics, railway geotechnics, nuclear waste disposal, lime/cement stabilized soils, soil-vegetation-atmosphere interaction, compaction of agricultural soils, etc.